Mapping DNA Quantity into Electrophoretic Mobility through Quantum Dot Nanotethers for High-Resolution Genetic and Epigenetic Analysis

Yi Zhang,[†,⊥] Kelvin J. Liu,[§] Tian-Li Wang,[⊥] Ie-Ming Shih,[‡,⊥] and Tza-Huei Wang[†,§,⊥,∥,*]

[†]Department of Biomedical Engineering, Johns Hopkins University School of Medicine, Baltimore, Maryland 21205, United States, [‡]Department of Pathology, The Johns Hopkins University School of Medicine, Baltimore, Maryland 21231, United States, [§]Department of Mechanical Engineering, Johns Hopkins University, Baltimore, Maryland 21218, United States, [⊥]Sidney Kimmel Comprehensive Cancer Center at Johns Hopkins, Baltimore, Maryland 21287, United States, and [∥]Center of Cancer Nanotechnology Excellence at the Johns Hopkins Institute for NanoBioTechnology, Johns Hopkins University, Baltimore, Maryland 21218, United States

ABSTRACT

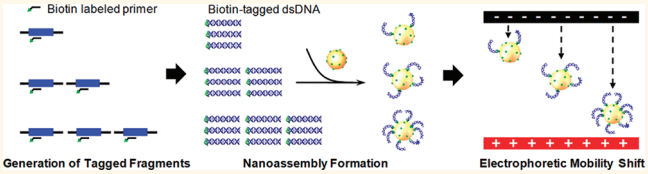

Newly discovered nanoparticle properties have driven the development of novel applications and uses. We report a new observation where the electrophoretic mobility of a quantum dot/DNA nanoassembly can be precisely modulated by the degree of surface DNA conjugation. By using streptavidin-coated quantum dots (QDs) as nanotethers to gather biotin-labeled DNA into electrophoretic nanoassemblies, the QD surface charge is modulated and transformed into electrophoretic mobility shifts using standard agarose gel electrophoresis. Typical fluorescent assays quantify based on relative intensity. However, this phenomenon uses a novel approach that accurately maps DNA quantity into shifts in relative band position. This property was applied in a QD-enabled nanoassay called quantum dot electrophoretic mobility shift assay (QEMSA) that enables accurate quantification of DNA targets down to 1.1-fold (9%) changes in quantity, beyond what is achievable in qPCR. In addition to these experimental findings, an analytical model is presented to explain this behavior. Finally, QEMSA was applied to both genetic and epigenetic analysis of cancer. First, it was used to analyze copy number variation (CNV) of the *RSF1/HBXAP* gene, where conventional approaches for CNV analysis based on comparative genomic hybridization (CGH), microarrays, and qPCR are unable to reliably differentiate less than 2-fold changes in copy number. Then, QEMSA was used for DNA methylation analysis of the *p16/CDK2A* tumor suppressor gene, where its ability to detect subtle changes in methylation was shown to be superior to that of qPCR.

KEYWORDS: quantum dot · nanotether · DNA · electrophoretic mobility · copy number variation · DNA methylation

Quantum dots (QDs) have well-known optical properties including narrow emission spectra, high quantum yields, and high photostability that have made them very popular as passive fluorescent reporters in cell staining, *in vivo* imaging, and immunoassays.[1−3] Newly discovered properties and phenomena have often led to their incorporation as active participants in novel nanosensing and signal transduction mechanisms. For example, nonradioactive energy transfer can occur between a QD donor and an organic fluorophore acceptor in a phenomenon called quantum dot fluorescence resonance energy transfer (QD-FRET).[4] QD-FRET was among the first active signal transduction mechanisms which used QDs to create highly sensitive nanosensors for DNA mutation[5] and methylation anaylsis,[6] protein detection,[7] and biophysical studies.[8] Other phenomena, such as photoblinking,[9] were first thought of as limitations,[10] but further study of these properties has led to increased understanding of quantum dot photophysics and even the suggestion of new sensing mechanisms.[11] Indeed, recent reports of quantum dot participation in new phenomena such as multiexciton generation,[12] nanoantenna-directed emission,[13] and single photon emission[14] could lead to significant future advances in photodetection, nanosensing, and optical telecommunication.

We report a new phenomenon where the electrophoretic mobility of a QD−DNA nanoassembly can be precisely and predictably modulated by the degree of surface DNA conjugation. This phenomenon forms the basis of a nanoassay called quantum dot electrophoretic mobility shift assay (QEMSA) that is able to accurately quantify DNA using simple slab gel electrophoresis. Whereas electrophoretic mobility shift assays are most commonly used to investigate DNA−protein binding interactions, here they are used for precise DNA quantification. However, rather

* Address correspondence to thwang@jhu.edu.

Received for review November 11, 2011 and accepted December 3, 2011.

Published online December 03, 2011
10.1021/nn204377k

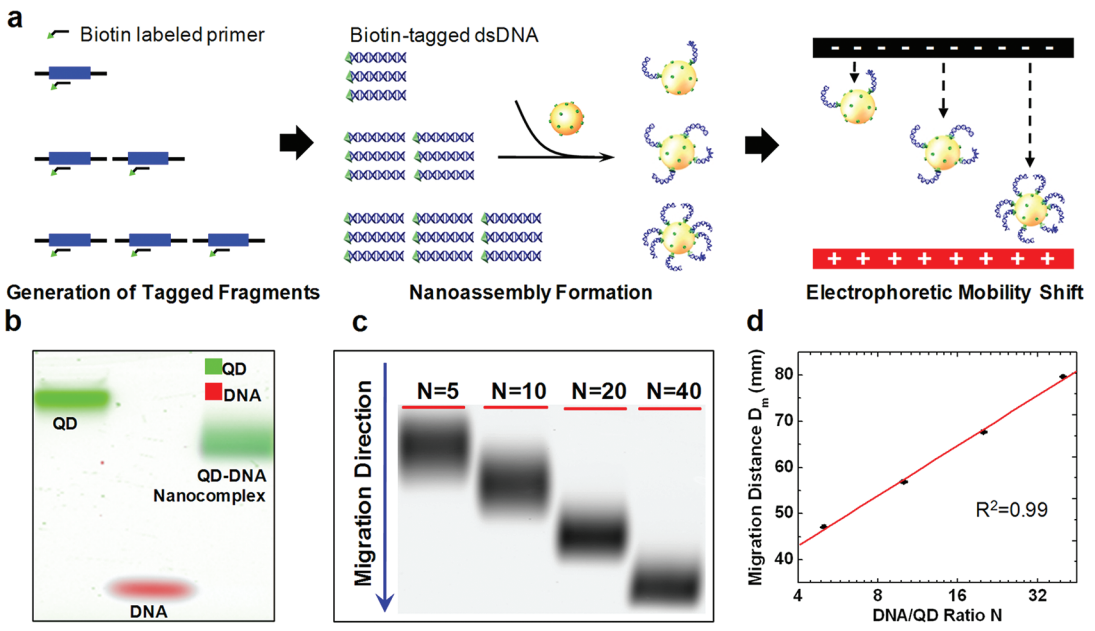

Figure 1. QEMSA working principle. (a) Biotin-tagged DNA fragments were generated from genomic DNA targets using biotinylated primers and a limited number of amplification cycles to preserve genomic DNA quantity information. The biotinylated DNA fragments were then mixed with streptavidin-coated QDs, and self-assembly would occur to form nanocomplexes where the resultant DNA:QD ratio, *N*, was dependent on the amount of input DNA. The electrophoretic mobility of the nanocomplexes increased with the DNA:QD ratio and was used to determine DNA quantity. (b) Pseudocolor gel image reveals that the QD−DNA nanocomplexes (combined green and red) migrated faster than the naked QDs (green) but slower than the oligonucleotides alone (red). (c) Representative gel image of QD−DNA nanocomplexes with various *N* values migrating in an agarose gel. The nanocomplexes with the largest *N* migrate fastest and *vice versa*. (d) Migration curve was obtained by plotting the migration distance of each gel band against the respective DNA:QD ratio, *N*. The migration distance was determined by measuring the point at which the leading edge of the electropherogram met the baseline intercept.

than quantifying based on band intensity, QEMSA maps DNA quantity into an electrophoretic mobility shift. Each streptavidin-functionalized QD acts as an electrophoretic nanotether, gathering biotin-tagged DNA from solution to form a QD−DNA nanoassembly. DNA amount is determined by measuring the relative speed at which the QD−DNA nanoassemblies migrate within the gel (*i.e.*, relative band position) relative to unconjugated QDs. First, the fundamental shift in electrophoretic mobility was experimentally explored, and a theoretical underpinning was derived. Then, the phenomenon was applied to genetic and epigenetic analysis of cancer where QEMSA enabled accurate quantification of gene copy number variation and promoter hypermethylation in cancer cells with greater resolution than existing real-time quantitative PCR (qPCR) methods.

RESULTS AND DISCUSSION

In QEMSA, the electrophoretic mobility of the QD−DNA nanoassembly is modulated by the degree of surface DNA conjugation (Figure 1a). In the absence of DNA, the streptavidin-functionalized QDs have low electrophoretic mobility and migrate slowly through the gel matrix under an applied electric field. However, in the presence of biotin-tagged DNA, the QDs capture these DNA strands, increasing their effective electrophoretic mobility and propelling the QD−DNA assemblies to migrate through the gel matrix at a faster rate (Figure 1b). Intuitively, the greater the number of conjugated DNA molecules, the faster the nanoassemblies migrate, thereby mapping DNA quantity into an electrophoretic mobility shift. To perform QEMSA, biotin-tagged DNA fragments are generated and duplicated from target gene sequences of genomic DNA using biotinylated probes. Streptavidin-coated quantum dots were then introduced so that the gene-specific biotinylated DNA fragments self-assembled onto the QD surface through the streptavidin−biotin interactions, forming QD−DNA nanocomplexes.

The rate at which the nanoassemblies migrate is then proportional to the number of DNA bound to each QD (*i.e.*, DNA:QD ratio, *N*). The dependence of migration distance, D_m, on *N* can be analytically derived as (Discussion, Supporting Information):

$$D_m = C_0 E t \times f(K_r, \iota, R) \ln N + M_0 \quad (1)$$

where *E* and *t* are the electrical field strength and migration time, respectively. C_0 and M_0 are constants relating to the temperature, buffer viscosity, ionic strength, and other environmental parameters. The term $f(K_r,\iota,R)$ describes the interaction of the QD−DNA nanocomplexes with the gel matrix, where K_r is the retardation factor, ι is the gel concentration, and *R* is the hydrodynamic radius of the nanocomplex.

TABLE 1. Zeta-Potentials and Hydrodynamic Radii of QD−DNA Nanocomplexes

DNA:QD ratio (*N*)	radius (nm)	zeta-potential (mV) at pH 7.4
0	10.11 ± 0.34	−5.81 ± 2.36
10	10.20 ± 0.74	−14.33 ± 1.15
20	10.40 ± 0.89	−15.97 ± 1.05
40	11.09 ± 0.30	−17.63 ± 2.55

The nanoassembly surface charge increases as the DNA:QD ratio increases, leading to greater electrophoretic force. Interestingly, minimal increases in hydrodynamic radius are seen as DNA binding increases. This was confirmed by examining the experimentally determined zeta-potential and hydrodynamic radius as function of DNA:QD ratio (Table 1). At neutral pH, the streptavidin-coated QDs only had a mild negative charge. Thus, the zeta-potential of the QD−DNA nanocomplex was dominated by the number of bound DNA molecules. Consequently, free QDs had low electrophoretic force and migrated slowly, whereas the nanoassemblies had higher electrophoretic force and migrated faster (Figure 1b). Free DNA migrated fastest as it was unrestrained by the QD nanotethers. On the basis of these results, R can be approximated as a constant in the case of QDs, and eq 1 can be reduced to

$$D_m \propto \ln N$$

When the previous experiment was repeated using streptavidin-coated polystyrene nanobeads in place of QDs, no shifts in electrophoretic mobility were seen (Figure S1, Supporting Information). The high intrinsic charge carried by the polystyrene itself masked the coupling of DNA to the nanobeads, and very little change in overall zeta-potential was seen. In addition to the low intrinsic charge, QDs are an ideal candidate for QEMSA for a two reasons. First, the QDs are small enough to freely migrate through the gel matrix. Second, the excellent optical properties of QDs make them ideal fluorescent reporters.[15] Hence, additional fluorophore labels are not required. These labels can otherwise affect the electrophoretic mobility of the nanocomplex and the log−linear dependence of the migration distance on the DNA:QD ratio (Figure S2, Supporting Information).

Figure 1c shows a representative gel image where a 2-fold serial dilution of DNA (strand *SO-1*, Table S1a, Supporting Information) was mixed with 10 nM QDs to form QD−DNA nanocomplexes with different N values. As predicted, the nanocomplex migration distance increased as N increased. The migration distance was determined by measuring the point at which the leading edge of the electropherogram met the baseline intercept. The migration distance was then plotted against the DNA:QD ratio to form a migration curve (Figure 1d). The strong correlation between N and D_m

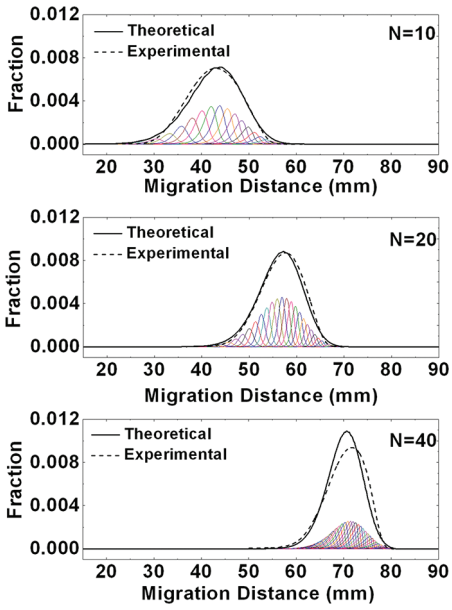

Figure 2. QEMSA band dispersion was seen to decrease with increasing values of N and increasing electrophoretic mobility. The gel was run at 8 V/cm. A theoretical model was used to simulate the Poissonian self-assembly process, and the theoretical band dispersion was calculated by summing all of the heterogeneous subpopulations (colored lines). The aggregate QEMSA band dispersions (black solid lines) are in good agreement with the experimental results (black dot lines) for N = 40, 20, and 10.

(R^2 = 0.99) suggests that the theoretical model accurately describes the QEMSA phenomenon.

Detailed examination of the gel images shows an interesting observation. In sharp contrast to standard gel electrophoresis, in QEMSA, bands with higher electrophoretic mobility appear sharper than bands with lower mobility. In order to explain this, the self-assembly of the QD−DNA nanocomplexes was modeled as a Poisson process[16] with an expectation value of N. Each gel band was the collective summation of all underlying subpopulations, where each subpopulation migrated at its own respective velocity (Figure 2) and the summation of which formed the final band. A numerical model based on this process and diffusive band broadening was used to calculate the expected band dispersion (Discussion, Supporting Information). As shown in the electropherograms in Figure 2, the numerical predictions agreed very well with the experimental results. Unlike a typical Poisson process where the variance increases linearly with the expectation value, the absolute band dispersion (*i.e.*, bandwidth) actually decreases as N increases. While the self-assembly of each QD−DNA nanocomplex behaves as a Poisson process, the migration distance of each subpopulation varies with ln N, thus greatly reducing the aggregate band dispersion for populations with high values of N.

Because differences in DNA quantity are readily transformed into variations in electrophoretic mobility, even subtle changes in DNA quantity can be reliably

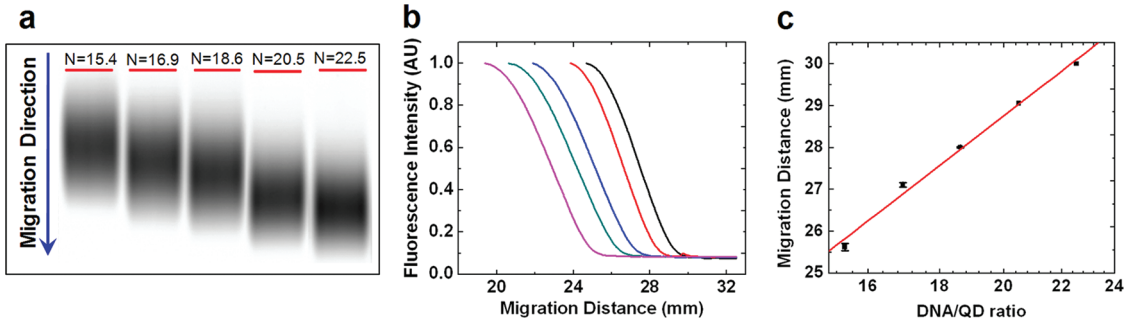

Figure 3. QEMSA was used to precisely distinguish ~9% differences in DNA copy number. The gel was run at 6 V/cm. (a) Raw gel image and (b) electropherogram (leading edge only) demonstrate resolution of a 1.1-fold DNA dilution series. (c) Standard migration curve of the 1.1-fold serially diluted DNA strands shows easily quantified differences in migration distance.

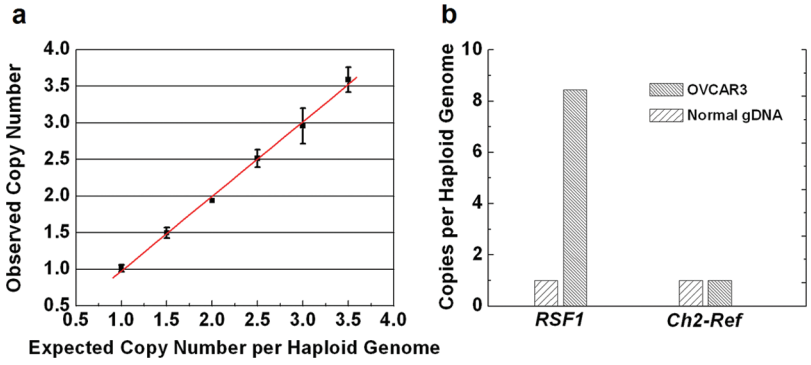

Figure 4. QEMSA was used to perform CNV analysis in OVCAR3 ovarian cancer cells. (a) Detection of *RSF1/HBXAP* copy number amplification using samples that mimic 2 to 7 copies per cell (1 to 3.5 copies per haploid genome). The *x*-axis shows the expected ratio of *RSF1/HBXAP* to the reference sequence, while the *y*-axis shows the ratio observed using QEMSA. (b) Reference sequence was unamplified in both the normal and cancerous cell lines. *RSF1/HBXAP* was found to be unamplified in the normal 2516 cells but amplified ~8.5-fold cancerous OVCAR3 cells.

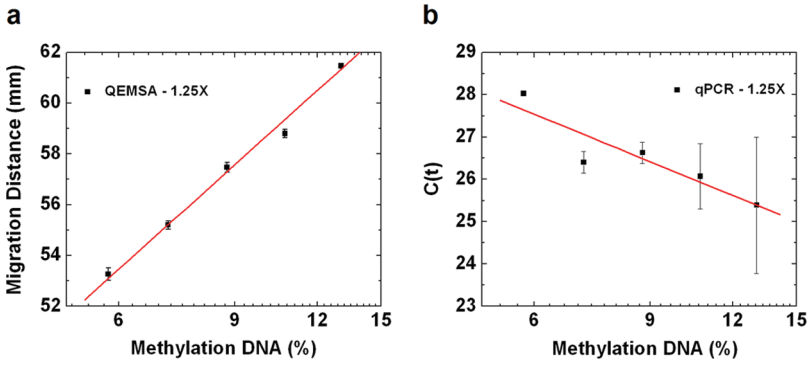

Figure 5. QEMSA was used to analyze promoter hypermethylation of the *p16/CDKN2A* gene. (a) Standard migration curve was created for serially diluted methylated genomic DNA with dilution factors of 1.25-fold. To simulate clinical samples, all methylated samples in the dilution series were spiked with 100 ng of unmethylated genomic DNA. Both the methylated and unmethylated DNA samples were then bisulfite treated and subject to analysis *via* QEMSA or qPCR. (b) Same dilution series were analyzed by qPCR. Due to the small dilution factors, the dilution series could not be reliably quantified with qPCR.

detected by enhancing this variation in the migration distance. As can be seen from eq 1, the enhancement effect can be achieved by increasing the electric field strength, increasing the electrophoresis time, and/or decreasing the gel concentration (Figure S3 and Table S2, Supporting Information). After optimizing these parameters, QEMSA was used to analyze 1.1-fold serially diluted DNA (Figure 3). Even such small differences in DNA quantity were transformed into easily measured differences in migration distance, demonstrating the ability to resolve as little as ~9% differences in quantity.

qPCR is considered the gold standard method for many forms of genetic analysis. While it has high sensitivity and wide dynamic range, it has difficulty distinguishing less than 2-fold differences[17−19] in quantity. The analysis of many biomarkers requires

the ability to distinguish subtle changes in level that may signal the early onset or severity of disease. QEMSA is used to analyze two such markers, DNA copy number variation (CNV) and DNA methylation, where current qPCR-based methods are unable to achieve this level of discrimination. DNA copy number variation (CNV) is a mutation where large regions of a chromosome (kb to Mb in size) are deleted, amplified, or inserted elsewhere. These regions often encompass entire genes and their regulatory regions,[20−24] leading to phenotypic changes by gene disruption or increased gene dosage.[25−27] Thus, the ability to accurately measure variations in DNA copy number may enable discrimination of cancer phenotype or prediction of therapeutic response.[28] Whereas qPCR is unable to resolve less than 2-fold changes in quantity (*i.e.*, 2 *vs* 4 copies), it is thought that even subtle changes in DNA copy number (*i.e.*, 4 *vs* 5 copies) can have great diagnostic and prognostic value. For example, it has been reported that changes in *HER2* copy number correlate with tumor aggressiveness in breast cancer and that anti-*HER2* therapy (*e.g.*, Herceptin) may be more effective in highly amplified tumors.[29]

As an initial validation, QEMSA was used to analyze copy number amplification of the *RSF1/HBXAP* gene in OVCAR3 ovarian carcinoma cells. *RSF1/HBXAP* is a chromatin remodeling gene that participates in transcriptional activation and repression. Studies have shown good correlation between *RSF1/HBXAP* gene amplification and ovarian cancer aggressiveness. The overall survival of ovarian cancer patients with *RSF1/HBXAP* amplification was generally shorter than those without,[30] suggesting that copy number amplification of *RSF1/HBXAP* can be a prognostic indicator of the disease severity, as well as a potential biomarker for ovarian cancer diagnosis.

In order to reliably quantify *RSF1/HBXAP* copy number amplification, a reference sequence was selected from a highly conserved region of the genome (Ch2-ref).[30] The reference sequence consistently maintained its copy number at 2 copies per cell (1 copy per haploid genome). *RSF1/HBXAP* copy number was then determined by examining the ratio between *RSF1/HBXAP* and Ch2-ref to eliminate inaccuracy caused by variations in DNA input. An *RSF1/HBXAP*:Ch2-ref ratio of 1 represents no amplification. A single duplication on one allele results in a total of 3 copies and a ratio of 1.5. A spiking experiment was first performed to test the resolution of QEMSA for CNV analysis. *RSF1/HBXAP* DNA fragments were mixed with Ch2-ref DNA fragments in ratios of 1, 1.5, 2, 2.5, 3, and 3.5 to simulate 2, 3, 4, 5, 6, and 7 copies per cell, respectively. In Figure 4a, a strong linear correlation was seen between the measured copy number per haploid and the expected copy number ($R^2 = 0.99$).

To determine *RSF1/HBXAP* copy number of the OVCAR3 cells, migration curves for *RSF1/HBXAP* and Ch2-ref were generated using serial dilutions of normal DNA obtained from 2516 cells with no *RSF1/HBXAP* amplification[30] to form standard curves. The OVCAR3 *RSF1/HBXAP* and Ch2-ref migration distances were then compared against these standard curves to determine the final copy number. It was found that the OVCAR3 cells had ~8.5-fold amplification of the *RSF1/HBXAP* gene (Figure 4b). This agrees well with previous results determined by SNP array.[30]

DNA methylation is an epigenetic modification that often occurs in the promoter regions of tumor suppressor and oncogenes. Thus, it is a promising biomarker for cancer detection and monitoring.[31−34] The ability to discriminate subtle changes in methylation is particularly important in highly heterogeneous samples such as cell-free nucleic acids, where small changes in methylated tumor DNA level can be masked by high background levels of unmethylated, healthy DNA.

QEMSA was used to quantify DNA methylation and compared against the gold standard qPCR method. A 1.25-fold dilution series of methylated genomic DNA was spiked into a background of unmethylated genomic DNA to simulate clinical samples comprising 6−13% methylated DNA. The samples first underwent bisulfite treatment[6,35] and then methylation specific PCR[36] to selectively produce biotin-tagged amplicons from the methylated *p16/CDK2A* promoter region. Amplification was stopped while still in the log−linear range, and QEMSA was used to quantify the biotin-tagged amplicons. In Figure 5a, the expected log−linear dependence between migration distance and DNA methylation level is seen. Accurate quantification of 1.25-fold changes in methylation was robustly obtained. As a comparison, when the same samples were also analyzed using qPCR, the results showed large variations and poor correlation between threshold cycles and DNA methylation level (Figure 5b).

CONCLUSION

In this report, we describe a phenomenon where the electrophoretic mobility of a QD−DNA nanoassembly can be precisely and predictably tuned by the level of surface DNA conjugation. Conventionally, the high sizing resolution of electrophoresis makes it a vital tool for molecular separation and binding analysis. Here, this phenomenon was used to perform QEMSA, an assay which transforms DNA quantity into shifts in gel band position. QDs were used as nanotethers to gather to target DNA strands into nanocomplexes where their electrophoretic mobility could be used to precisely determine the quantity of bound DNA. QEMSA was able to resolve ~9% differences in DNA amount. This level of resolution has not been previously achieved by any other quantification method including qPCR or nanofluidic digital PCR.[37] The capability of QEMSA in

differentiating integer copies of specific genes was demonstrated by detecting *RSF1/HBXAP* gene amplification in ovarian carcinoma cell lines. This gene-specific detection of CNV with high resolution is of paramount clinical importance.[30,38−40] We also demonstrated the use of QEMSA for quantifying methylation of a tumor suppressor gene, *p16/CDK2A*. QEMSA's enhanced resolution over qPCR offers an accurate means to measure methylation changes in cancer patients, a promising marker for patient therapeutic response.[41] In addition to the demonstrated assays, QEMSA can be easily extended to other genetic or epigenetic biomarkers where high quantification resolution is necessary.

METHODS

QD−DNA Nanocomplex Self-Assembly. The synthetic oligonucleotide *SO-1* was biotinylated at the 5′ terminal. *SO-2* was biotinylated at the 3′ terminal and labeled with Cy5 at the 5′ terminal (Table S1a). Streptavidin-coated QDs were diluted to 10 nM in buffer containing 10 mM Tris and 10 mM NaCl at pH 7.4. The diluted QDs were mixed with oligonucleotide of the desired concentrations at 1:1 volume ratio. Hence, the final QD concentration was 5 nM. For 10 μL reaction volume, the 2-fold serial dilution starts with the highest DNA quantity of 12.9 ng, and the 1.1-fold serial dilution starts with the highest DNA quantity of 7.25 ng. The mixture was shielded from light and incubated at room temperature for 1 h. Ten microliters of QD−DNA nanocomplexes was then loaded onto the agarose gel for QEMSA analysis.

Gel Imaging. The gels were scanned on a Typhoon 9400 variable mode imager. For QD605 imaging, a 488 nm laser and 610BP30 emission filter were used with a gain of 500 and high sensitivity setting. For Cy5, a 633 nm laser and 670BP30 emission filter were used with a gain of 400 and high sensitivity setting.

gDNA and Cell Line Preparation. An ovarian cancer cell line, OVCAR3, was obtained from the American Tissue Culture Center (Rockville, Maryland) and a primary culture, 2516, was established from a normal fallopian tube epithelium. Cells were cultured in RPMI1640 supplemented with 10% fetal bovine serum. Genomic DNA was prepared from both cell cultures using a Qiagen blood DNA extraction kit and the accompanying protocol.

Analysis of Copy Number Amplification of the *RSF1/HBXAP* Gene in OVCAR3 Using QEMSA. The gDNA was first subject to PCR with limited amplification (Table S3a) using a biotinylated primer. This allowed amplification of the target sequence while preserving the relative levels of input DNA. The reaction was then digested with exonuclease I to remove the excess single-stranded biotinylated primer which could compete with the target sequence upon binding to the QD and affect the electrophoretic mobility of the resultant QD−DNA nanocomplex. To generate the *RSF1/HBXAP* standard migration curve, 2-fold serially diluted gDNA from the normal cell line (2516), with 7.5 ng initial level, was amplified in a 25 μL reaction containing 67 mM Tris, 16.6 mM ammonium sulfate, 6.7 mM $MgCl_2$, 10 nM 2-mercaptoethanol, 0.1 unit/μL *Taq* polymerase, 600 μM of each deoxynucleotide, and 500 nM of primer *Rsf-S*. The forward primer was conjugated with biotin (Table S1b). The reaction was performed by thermal cycling according to the recipe shown in Table S3a. Then each sample was treated with 20 units of exonuclease I at 37 °C for 2 h. Last, the biotin-tagged amplicons were mixed with 20 nM QD at 1:1 volume ratio and incubated at the room temperature for 1 h. The QD−DNA nanocomplex self-assembled during the incubation, and 10 μL of the nanocomplexes was analyzed using QEMSA. The standard migration curve for the reference sequence was generated using the same dilution series and the same procedure except with *Ch2-ref-S* primers (Table S1b).To determine OVCAR3 *RSF1/HBXAP* copy number amplification, the *RSF1/HBXAP* gene and the reference sequence of the cancerous gDNA samples were amplified to produce biotinylated fragments, analyzed with QEMSA, and compared to the standard migration curves.

CNV Spike-In Experiment Using QEMSA. Using primers *Rsf-T* and *Ch2-ref-T* (Table S1b), two DNA fragments were generated from the *RSF1/HBXAP* gene and the reference sequence by PCR (Table S3b). The fragments were treated with exonuclease I to remove all of the excess primers and purified twice with QIAquick PCR purification kit. The two purified fragments were quantified using a UV/vis spectrophotometer and mixed at desired ratios. The fragments were then tagged with biotin using the PCR recipe shown in Table S3c, and the QEMSA analysis was performed using the aforementioned procedure.

Quantification of DNA Methylation. Unmethylated genomic DNA was isolated from the normal leukocytes obtained from healthy individuals after receiving informed consent. Methylated gDNA was obtained by treating the normal genomic DNA with *SSSI* methyltransferase. Both normal and methylated gDNA were bisulfite treated (text S1, Methods), quantified *via* absorbance using a NanoDrop and stored at −20 °C until use. The 1.25-fold dilution series of methylated gDNA, starting from 15 ng, was spiked into 100 ng of normal gDNA. Methylation specific primer p16 M (Table S1b) only targets the methylated promoter region of the *p16/CDKN2A* gene. Hence, p16 M was introduced to selectively amplify the methylated gDNA in the presence of unmethylated gDNA using MSP (Table S3d). Each 25 μL reaction contained 67 mM Tris, 16.6 mM ammonium sulfate, 6.7 mM $MgCl_2$, 10 nM 2-mercaptoethanol, and 0.1 unit/μL HotStart *Taq* polymerase, 1.25 mM of each deoxynucleotides and 300 nM of primers. QEMSA analysis was subsequently performed on the biotin-tagged amplicons using aforementioned procedure.

Acknowledgment. The authors would like to thank Dr. H.Q. Mao and Mr. Y. Ren for helping with the zeta-potentiometry and dynamic light scattering measurement. We also would like to thank Miss N. Bhise and Mr. T. Rane for helping with the particle imaging velocimetry. The authors would like to express their appreciation to the support from NIH (R21CA120742, R01CA1 55305, U54CA151838, P50CA058184, and R01CA129080), AACR Stand Up To Cancer (SU2C-AACR-CT0109) and NSF (0546012, 0730503, 0725528, 0967375). Y.Z. would like to thank the funding support from Hodson Trust.

Supporting Information Available: Supporting discussion contains the detailed derivation of QEMSA governing equation. Supporting methods include materials, instrument, and protocol for bisulfite treatment. Additional results and protocols are presented in supporting figures and tables. This material is available free of charge *via* the Internet at http://pubs.acs.org.

REFERENCES AND NOTES

1. Medintz, I. L.; Uyeda, H. T.; Goldman, E. R.; Mattoussi, H. Quantum Dot Bioconjugates for Imaging, Labelling and Sensing. *Nat. Mater.* **2005**, *4*, 435–446.
2. Michalet, X.; Pinaud, F. F.; Bentolila, L. A.; Tsay, J. M.; Doose, S.; Li, J. J.; Sundaresan, G.; Wu, A. M.; Gambhir, S. S.; Weiss, S. Quantum Dots for Live Cells, *In Vivo* Imaging, and Diagnostics. *Science* **2005**, *307*, 538–544.
3. Smith, A. M.; Duan, H.; Mohs, A. M.; Nie, S. Bioconjugated Quantum Dots for *In Vivo* Molecular and Cellular Imaging. *Adv. Drug Delivery Rev.* **2008**, *60*, 1226–1240.
4. Willard, D. M.; Carillo, L. L.; Jung, J.; Van Orden, A. CdSe−ZnS Quantum Dots as Resonance Energy Transfer

Donors in a Model Protein−Protein Binding Assay. *Nano Lett.* **2001**, *1*, 469–474.
5. Zhang, C. Y.; Yeh, H. C.; Kuroki, M. T.; Wang, T. H. Single-Quantum-Dot-Based DNA Nanosensor. *Nat. Mater.* **2005**, *4*, 826–831.
6. Bailey, V. J.; Easwaran, H.; Zhang, Y.; Griffiths, E.; Belinsky, S. A.; Herman, J. G.; Baylin, S. B.; Carraway, H. E.; Wang, T. H. MS-qFRET: A Quantum Dot-Based Method for Analysis of DNA Methylation. *Genome Res.* **2009**, *19*, 1455–1461.
7. Medintz, I. L.; Clapp, A. R.; Mattoussi, H.; Goldman, E. R.; Fisher, B.; Mauro, J. M. Self-Assembled Nanoscale Biosensors Based on Quantum Dot FRET Donors. *Nat. Mater.* **2003**, *2*, 630–638.
8. Chen, H. H.; Ho, Y. P.; Jiang, X.; Mao, H. Q.; Wang, T. H.; Leong, K. W. Quantitative Comparison of Intracellular Unpacking Kinetics of Polyplexes by a Model Constructed from Quantum Dot-FRET. *Mol. Ther.* **2008**, *16*, 324–332.
9. Kuno, M.; Fromm, D. P.; Hamann, H. F.; Gallagher, A.; Nesbitt, D. J. Nonexponential "Blinking" Kinetics of Single CdSe Quantum Dots: A Universal Power Law Behavior. *J. Chem. Phys.* **1999**, *112*, 3117–3120.
10. Hohng, S.; Ha, T. Near-Complete Suppression of Quantum Dot Blinking in Ambient Conditions. *J. Am. Chem. Soc.* **2004**, *126*, 1324–1325.
11. Hammer, N. I.; Early, K. T.; Sill, K.; Odoi, M. Y.; Emrick, T.; Barnes, M. D. Coverage-Mediated Suppression of Blinking in Solid State Quantum Dot Conjugated Organic Composite Nanostructures. *J. Phys. Chem. B* **2006**, *110*, 14167–14171.
12. Sukhovatkin, V.; Hinds, S.; Brzozowski, L.; Sargent, E. H. Colloidal Quantum-Dot Photodetectors Exploiting Multiexciton Generation. *Science* **2009**, *324*, 1542–1544.
13. Curto, A. G.; Volpe, G.; Taminiau, T. H.; Kreuzer, M. P.; Quidant, R.; van Hulst, N. F. Unidirectional Emission of a Quantum Dot Coupled to a Nanoantenna. *Science* **2010**, *329*, 930–933.
14. Claudon, J.; Bleuse, J.; Malik, N. S.; Bazin, M.; Jaffrennou, P.; Gregersen, N.; Sauvan, C.; Lalanne, P.; Gerard, J.-M. A Highly Efficient Single-Photon Source Based on a Quantum Dot in a Photonic Nanowire. *Nat. Photonics* **2010**, *4*, 174–177.
15. Resch-Genger, U.; Grabolle, M.; Cavaliere-Jaricot, S.; Nitschke, R.; Nann, T. Quantum Dots *versus* Organic Dyes as Fluorescent Labels. *Nat. Methods* **2008**, *5*, 763–775.
16. Pons, T.; Medintz, I. L.; Wang, X.; English, D. S.; Mattoussi, H. Solution-Phase Single Quantum Dot Fluorescence Resonance Energy Transfer. *J. Am. Chem. Soc.* **2006**, *128*, 15324–15331.
17. Bubner, B.; Gase, K.; Baldwin, I. T. Two-Fold Differences Are the Detection Limit for Determining Transgene Copy Numbers in Plants by Real-Time PCR. *BMC Biotechnol.* **2004**, *4*, 14.
18. Lo, Y. M. D.; Lun, F. M. F.; Chan, K. C. A.; Tsui, N. B. Y.; Chong, K. C.; Lau, T. K.; Leung, T. Y.; Zee, B. C. Y.; Cantor, C. R.; Chiu, R. W. K. Digital PCR for the Molecular Detection of Fetal Chromosomal Aneuploidy. *Proc. Natl. Acad. Sci. U.S.A.* **2007**, *104*, 13116–13121.
19. Zimmermann, B.; Holzgreve, W.; Wenzel, F.; Hahn, S. Novel Real-Time Quantitative PCR Test for Trisomy 21. *Clin. Chem.* **2002**, *48*, 362–363.
20. Iafrate, A. J.; Feuk, L.; Rivera, M. N.; Listewnik, M. L.; Donahoe, P. K.; Qi, Y.; Scherer, S. W.; Lee, C. Detection of Large-Scale Variation in the Human Genome. *Nat. Genet.* **2004**, *36*, 949–951.
21. Sebat, J.; Lakshmi, B.; Troge, J.; Alexander, J.; Young, J.; Lundin, P.; Maner, S.; Massa, H.; Walker, M.; Chi, M. Y.; *et al.* Large-Scale Copy Number Polymorphism in the Human Genome. *Science* **2004**, *305*, 525–528.
22. Sharp, A. J.; Cheng, Z.; Eichler, E. E. Structural Variation of the Human Genome. *Annu. Rev. Genomics Hum. Genet.* **2006**, *7*, 407–442.
23. Sharp, A. J.; Locke, D. P.; McGrath, S. D.; Cheng, Z.; Bailey, J. A.; Vallente, R. U.; Pertz, L. M.; Clark, R. A.; Schwartz, S.; Segraves, R.; *et al.* Segmental Duplications and Copy-Number Variation in the Human Genome. *Am. J. Hum. Genet.* **2005**, *77*, 78–88.
24. Tuzun, E.; Sharp, A. J.; Bailey, J. A.; Kaul, R.; Morrison, V. A.; Pertz, L. M.; Haugen, E.; Hayden, H.; Albertson, D.; Pinkel, D.; *et al.* Fine-Scale Structural Variation of the Human Genome. *Nat. Genet.* **2005**, *37*, 727–732.
25. Buckland, P. R. Polymorphically Duplicated Genes: Their Relevance to Phenotypic Variation in Humans. *Ann. Med.* **2003**, *35*, 308–315.
26. Nguyen, D. Q.; Webber, C.; Ponting, C. P. Bias of Selection on Human Copy-Number Variants. *PLoS Genet.* **2006**, *2*, 198–207.
27. Repping, S.; van Daalen, S. K. M.; Brown, L. G.; Korver, C. M.; Lange, J.; Marszalek, J. D.; Pyntikova, T.; van der Veen, F.; Skaletsky, H.; Page, D. C.; *et al.* High Mutation Rates Have Driven Extensive Structural Polymorphism Among Human Y Chromosomes. *Nat. Genet.* **2006**, *38*, 463–467.
28. McCaughan, F. Molecular Copy-Number Counting: Potential of Single-Molecule Diagnostics. *Expert Rev. Mol. Diagn.* **2009**, *9*, 309–312.
29. Lambein, K.; Praet, M.; Forsyth, R.; Van den Broecke, R.; Braems, G.; Matthys, B.; Cocquyt, V.; Denys, H.; Pauwels, P.; Libbrecht, L. Relationship between Pathological Features, HER2 Protein Expression and *HER2* and *CEP17* Copy Number in Breast Cancer: Biological and Methodological Considerations. *J. Clin. Pathol.* **2010**, *64*, 200–207.
30. Shih, L. M.; Sheu, J. J. C.; Santillan, A.; Nakayama, K.; Yen, M. J.; Bristow, R. E.; Vang, R.; Parmigiani, G.; Kurman, K. E.; Trope, C. G.; *et al.* Amplification of a Chromatin Remodeling Gene, Rsf-1/HBXAP, in Ovarian Carcinoma. *Proc. Natl. Acad. Sci. U.S.A.* **2005**, *102*, 14004–14009.
31. Esteller, M.; Catasus, L.; Matias-Guiu, X.; Mutter, G. L.; Prat, J.; Baylin, S. B.; Herman, J. G. hMLH1 Promoter Hypermethylation Is an Early Event in Human Endometrial Tumorigenesis. *Am. J. Pathol.* **1999**, *155*, 1767–1772.
32. Feinberg, A. P.; Tycko, B. The History of Cancer Epigenetics. *Nat. Rev. Cancer* **2004**, *4*, 143–153.
33. Jones, P. A.; Baylin, S. B. The Fundamental Role of Epigenetic Events in Cancer. *Nat. Rev. Genet.* **2002**, *3*, 415–428.
34. Yamada, Y.; Jackson-Grusby, L.; Linhart, H.; Meissner, A.; Eden, A.; Lin, H.; Jaenisch, R. Opposing Effects of DNA Hypomethylation on Intestinal and Liver Carcinogenesis. *Proc. Natl. Acad. Sci. U.S.A.* **2005**, *102*, 13580–13585.
35. Bailey, V. J.; Keeley, B. P.; Zhang, Y.; Ho, Y. P.; Easwaran, H.; Brock, M. V.; Pelosky, K. L.; Carraway, H. E.; Baylin, S. B.; Herman, J. G.; *et al.* Enzymatic Incorporation of Multiple Dyes for Increased Sensitivity in QD-FRET Sensing for DNA Methylation Detection. *Chembiochem* **2010**, *11*, 71–74.
36. Herman, J. G.; Graff, J. R.; Myohanen, S.; Nelkin, B. D.; Baylin, S. B. Methylation-Specific PCR: A Novel PCR Assay for Methylation Status of CpG Islands. *Proc. Natl. Acad. Sci. U.S.A.* **1996**, *93*, 9821–9826.
37. Qin, J.; Jones, R. C.; Ramakrishnan, R. Studying Copy Number Variations Using a Nanofluidic Platform. *Nucleic Acids Res.* **2008**, *36*, e116.
38. Lupski, J. R. Genomic Rearrangements and Sporadic Disease. *Nat. Genet.* **2007**, *39*, S43–S47.
39. Meltzer, P. S., Kallioniemi, A.; Trent, J. M. *The Genetic Basis of Human Cancer*; McGraw-Hill: New York, 2002; pp 99−113.
40. Ropers, H. H. New Perspectives for the Elucidation of Genetic Disorders. *Am. J. Hum. Genet.* **2007**, *81*, 199–207.
41. Esteller, M.; Garcia-Foncillas, J.; Andion, E.; Goodman, S. N.; Hidalgo, O. F.; Vanaclocha, V.; Baylin, S. B.; Herman, J. G. Inactivation of the DNA-Repair Gene MGMT and the Clinical Response of Gliomas to Alkylating Agents. *N. Engl. J. Med.* **2000**, *343*, 1350–1354.